DOI: 10.1002/ejic.201100128

Imidozirconocene-Mediated Ring Cleavage of Epoxides – Evidence for Bifunctional Reactivity from DFT

Dhurairajan Senthilnathan[a] and Ponnambalam Venuvanalingam*[a]

Keywords: Epoxides / Zirconium / Sandwich complexes / Density functional calculations / Reaction mechanisms

The ring cleavage of epoxides mediated by bis(cyclopentadienyl)(*tert*-butylimido)zirconium (Cp_2Zr=N–*t*Bu)(THF) has been investigated using DFT calculations with a view to understand the mechanism of epoxide ring cleavage and the role of the imidozirconocene complex. Two types of epoxides have been chosen; some with and some without accessible β-hydrogen atoms. Epoxides without accessible β-hydrogen atoms undergo only insertion, whereas those with undergo both insertion and elimination. Although insertion is found to follow a zwitterionic mechanism, the elimination passes through a concerted intramolecular hydrogen transfer step. The role of the imidozirconocene complex has been elucidated by EDA and NBO analysis, which show that the vacant $1a_1$ molecular orbital of the Lewis acidic metal center of Cp_2Zr=N–*t*Bu fragment initiates the reaction as a Lewis acidic center and the Lewis basic imido nitrogen atom of the Cp_2Zr=N–*t*Bu fragment completes the reaction. The coordinate to covalent bond conversion and the involvement of the $1a_1$ and $2a_1$ molecular orbitals of the Cp_2Zr=N–*t*Bu fragment in the reaction have been examined. The formation of a five-membered metallacycle in the insertion and the alkoxy allyl product in the elimination predicted by calculations concur with experimental observations. Topological analysis has been carried out to further elucidate the mechanism and to reveal the bifunctional reactivity of imidozirconocene in epoxide ring opening reactions.

Introduction

Terminal transition metal imido compounds have attracted considerable interest for several decades and their role in organic transformations has been reviewed.[1–2] In particular, the chemistry of complexes with transition metals including zirconium,[3] iridium, rhodium, ruthenium,[4] and titanium have been extensively explored.[5–6] These complexes are known for their bifunctional reactivity with the metal center acting as a Lewis acid and the imido nitrogen atom as a Lewis base. Ring cleavage of epoxides using imidozirconocene is synthetically useful[7–14] and mechanistically challenging. Bergman and coworkers have studied these reactions extensively.[15] Imidozirconocene-mediated epoxide ring cleavages undergo insertion when epoxides do not have accessible β-hydrogen atoms and elimination when accessible β-hydrogen atoms are present.[15] In insertion, a metallacycle is formed, whereas an alkoxy allyl product is formed in the elimination process. Gansauer and coworkers have reported that titanocene-mediated epoxide ring cleavage preferentially follows a diradical mechanism.[16] These observations are experimentally proven but the mechanistic routes of these reactions are still unclear. Therefore, it is interesting to investigate the role of β-hydrogen atoms in the reaction. Furthermore, it is still unclear if the insertion passes through a zwitterionic or a diradical path as there are reports of both in the literature.[15,16–20] The bifunctional reactivity of imidozirconocene is also investigated. Thus, detailed computational studies on the mechanism of imidozirconocene-mediated epoxide ring opening reactions will offer new insights into its reactivity. This work addresses the following points: (i) the role of accessible β-hydrogen atoms in the mechanism, (ii) the bifunctional reactivity of imidozirconocene complexes and the electronic structure of the transition states, and (iii) the mechanism of the insertion reaction.

Computational Details

All computations have been carried out using Gaussian 03 software.[21] All calculations have been performed at B3LYP/LANL2DZ level[22] as this has been found to perform reasonably well by earlier studies on organometallic chemistry.[23–26] Zero point energies and thermal contributions to thermodynamic functions and activation parameters, as well as harmonic frequencies have been computed at the same level of theory on the optimized structures. Frequency calculations have been performed to confirm the nature of the stationary points, transition states (TSs) have one imaginary frequency and minima have real frequencies.[27] In order to characterize the bifunctional reactivity of imidozirconocene complex, natural bond order

[a] School of Chemistry, Bharathidasan University,
Tiruchirappalli 24, India
Fax: +91-431-2704045
E-mail: venuvanalingam@yahoo.com
Supporting information for this article is available on the WWW under http://dx.doi.org/10.1002/ejic.201100128.

 © 2011 Wiley-VCH Verlag GmbH & Co. KGaA, Weinheim

(NBO)[28–29] analyses have been performed using the NBO v. 3.1 module implemented in Gaussian 03.

In this computational study, the broken symmetry (BS) formalism proposed by Noodleman and coworkers[30] has been adopted for all diradical transition states and intermediate species. All the species with a diradical pathway have been optimized by using the STABLE = OPT keyword. This keyword coaxes Gaussian 03[21] to perform the stability analysis. If a restricted DFT solution is found to be unstable, the modification of STABLE by OPT induces G03 to automatically find an asymmetry to a symmetry broken DFT solution at a lower energy. This option produces symmetry broken guess orbitals by forming the plus and minus linear combinations of the symmetry adapted restricted frontier guess orbitals.[31] Using this symmetry broken guess orbital we obtained a symmetry DFT solution. Their energies were identical to the energies of the BS solutions obtained from the stability analysis. The observed energy $E_{(BS)}$ of the BS solution (SI-1) is very low with the lowest spin contamination $\langle S^2 \rangle$ for all the diradical transition sates and intermediates. This trend clearly explains the stable singlet diradical species in the ground state and there is no need for further spin projection formalism.[32]

In order to identify the bonding changes during the course of reaction, energy decomposition analyses (EDA) have been carried out for imidozirconocene complexes and insertion reaction intermediates at BP86/TZP level using the ADF 2007 package.[33–42] The detailed formalism of EDA is given in the Supporting Information. Furthermore, the bonding changes in the insertion reaction and the concerted mechanism of the elimination reaction and the bifunctional reactivity of imidozirconocene have been analyzed using the Laplacian of the charge density [$\nabla^2\rho(r)$] as well as by checking the presence of a bond path linking a pair of atoms (molecular graph) in the atoms in molecule (AIM) analysis using AIM2000.[43–46] The B3LYP/LANL2DZ wave function was used for the AIM analysis.

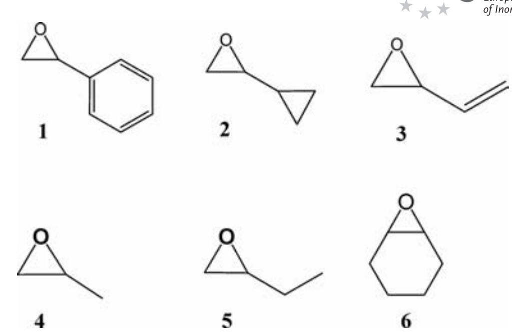

Figure 1. Epoxides **1**–**6** chosen for modeling the ring cleavage reaction mediated by imidozirconocene complex.

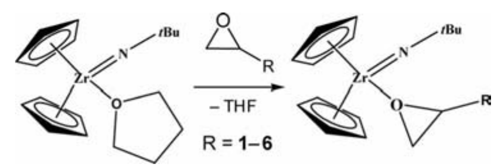

Scheme 1. Instantaneous replacement of THF from the imidozirconocene–THF complex by epoxide.

In the species name, the epoxide number (**1**–**6**) comes first and the insertion (I) or elimination (E) path is indicated next. TSs and intermediates are denoted as TS and Int. Zwitterionic and diradical species are denoted by zw and dr, respectively, as subscripts. For example **2**ITS1$_{zw}$ refers to the first TS species that occurs on the insertion path of **2** by the zwitterionic mechanism. Allyl alkoxy products that occur in the elimination paths are simply represented as *n*EP, where *n* is the epoxide number. The metallacycle products of insertion pathway are denoted as *n*MC(*m*) where *m* is the ring size. In the general scheme the epoxide number is dropped in the species name as the species are common to all epoxide reactions.

Results and Discussion

Two types of epoxide have been considered. The first type includes styrene oxide (**1**), vinylcyclopropane oxide (**2**), and butadiene monoepoxide (**3**), which do not have accessible β-hydrogen atoms. The second type includes propene oxide (**4**), butene oxide (**5**), and cyclohexene oxide (**6**), which have accessible β-hydrogen atoms (Figure 1). The imidozirconocene complex exists in tetrahydrofuran (THF) solution as a coordination complex with a THF group coordinated to Zr. When the epoxides are added the THF group is completely replaced by the epoxide even at very low temperatures (Scheme 1) due to the difference in oxophilicity between THF and the epoxides.[15] Therefore, the imidozirconocene epoxide complex is considered as a reactant throughout this study and it is this complex that undergoes ring cleavage.

Ring Cleavage of Epoxides without Accessible β-Hydrogen Atoms (1–3)

With ring cleavage, these epoxides mainly undergo insertion and there are no reports of elimination. Therefore only insertion is considered. The insertion can follow either a zwitterionic or a diradical mechanism. The overall mechanism for this reaction is described in Scheme 2.

Although these epoxides finally form five-membered metallacycles as products in the insertion reactions, the formation of an eight-membered metallacycle in the case of **2** and a seven-membered metallacycle in the case of **3** have been proposed.[15] These possibilities have been examined here (Scheme 2), and the relative free energy profiles for the reactions are presented in Figures 2, 3, and 4. The optimized geometries and selected bond lengths of TSs are presented in the Supporting Information, and key results are discussed here.

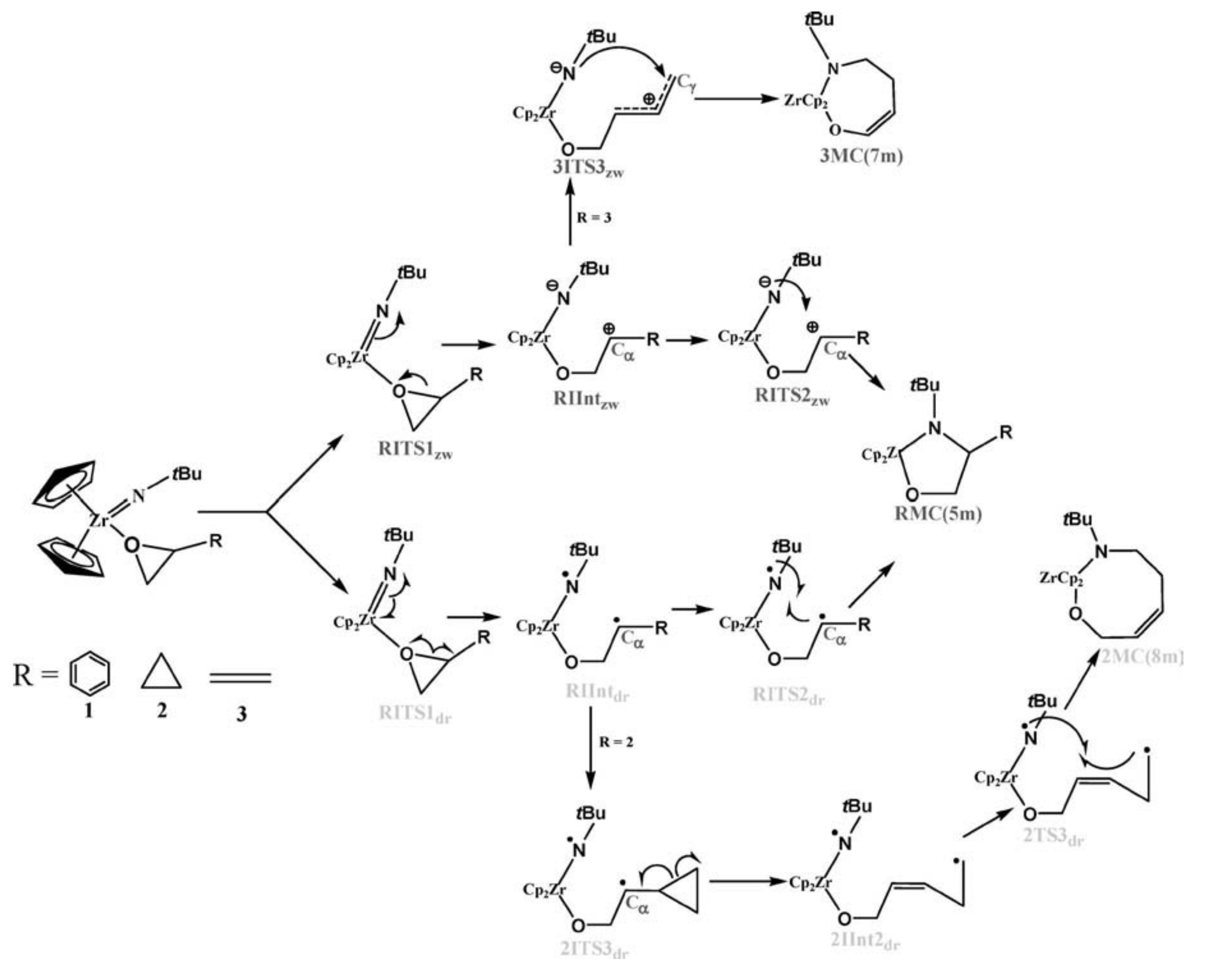

Scheme 2. Overall mechanism for the ring cleavage reactions of epoxides without accessible β-hydrogen atoms (R = **1**–**3**) mediated by imidozirconocene.

Styrene Oxide (1)

Initially the oxygen lone pair of the epoxide is donated to the zirconium atom to form a Zr←O coordinate bond. At the beginning of the reaction the C_α–O bond is cleaved either heterolytically or homolytically leading to zwitterionic or diradical intermediates, respectively (Scheme 2; R = 1).

The corresponding transitions states **1**ITS1$_{zw}$ and **1**ITS1$_{dr}$ differ only by 3.27 kcal/mol (Figure 2) with the zwitterionic path lying lower in energy. The TSs form their respective intermediates and in the intermediate (**1**IInt$_{zw}$ and **1**IInt$_{dr}$) the C_α–O bond is completely cleaved and the oxygen–zirconium coordinate bond (Zr←O) becomes a full covalent bond (Zr–O) as the zirconium–imido nitrogen π bond (Zr=N) is broken. The π bond electron pair becomes an additional lone pair on the nitrogen atom, which leads to the formation of a nucleophilic nitrogen atom in both the zwitterionic and diradical intermediates. In the zwitterionic intermediate, the Lewis basic nitrogen atom makes a nucleophilic attack (**1**ITS2$_{zw}$) on the carbocation (C_α) and forms a five-membered metallacycle [**1**MC(5m)]. The diradical intermediate (**1**IInt$_{dr}$) undergoes radical cyclization, through a barrier of 4.51 kcal/mol, forming the same five-membered metallacycle. Overall the zwitterionic path is low-lying due to the resonance stabilization of phenyl group compared to that of diradical path and the five-membered metallacycle is thermodynamically stable. The transition state geometries and bond lengths (SI-3) clearly indicate the breaking of the C_α–O and Zr=N π bonds and, in **1**ITS2, the formation of the N–C_α bond.

Vinylcyclopropane Oxide (2)

Scheme 2 (R = 2) shows that the cleavage of **2** passes through similar steps as discussed above and further in the radical path, the homolytic cleavage of cyclopropane in the **2**IInt$_{zw}$ ring can lead to the formation of an eight-membered metallacycle **2**MC(8m), which has been suggested by Bergmann and coworkers.[15]

The free energy profile of this reaction (Figure 3) shows that the zwitterionic mechanism is favorable and the five-membered metallacycle **2**MC(5m) is thermodynamically more stable. The formation of an eight-membered metallacycle **2**MC(8m) is ruled out as it is energetically highly unfavorable. Therefore the experimental observation[15] of a five-membered metallacycle is in agreement with the com-

 © 2011 Wiley-VCH Verlag GmbH & Co. KGaA, Weinheim

EurJIC European Journal of Inorganic Chemistry

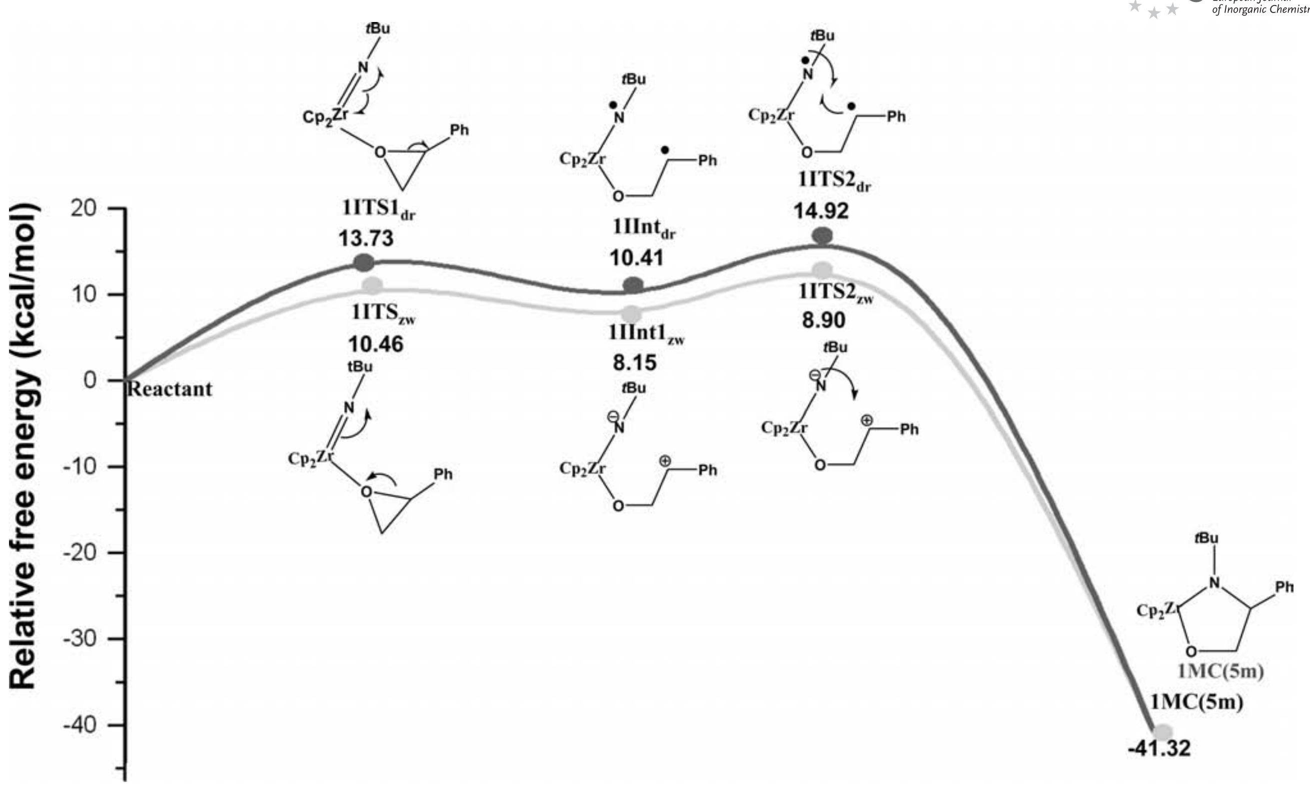

Figure 2. Free energy profile for the ring cleavage reaction of **1** mediated by the imidozirconocene complex at B3LYP/LANL2DZ.

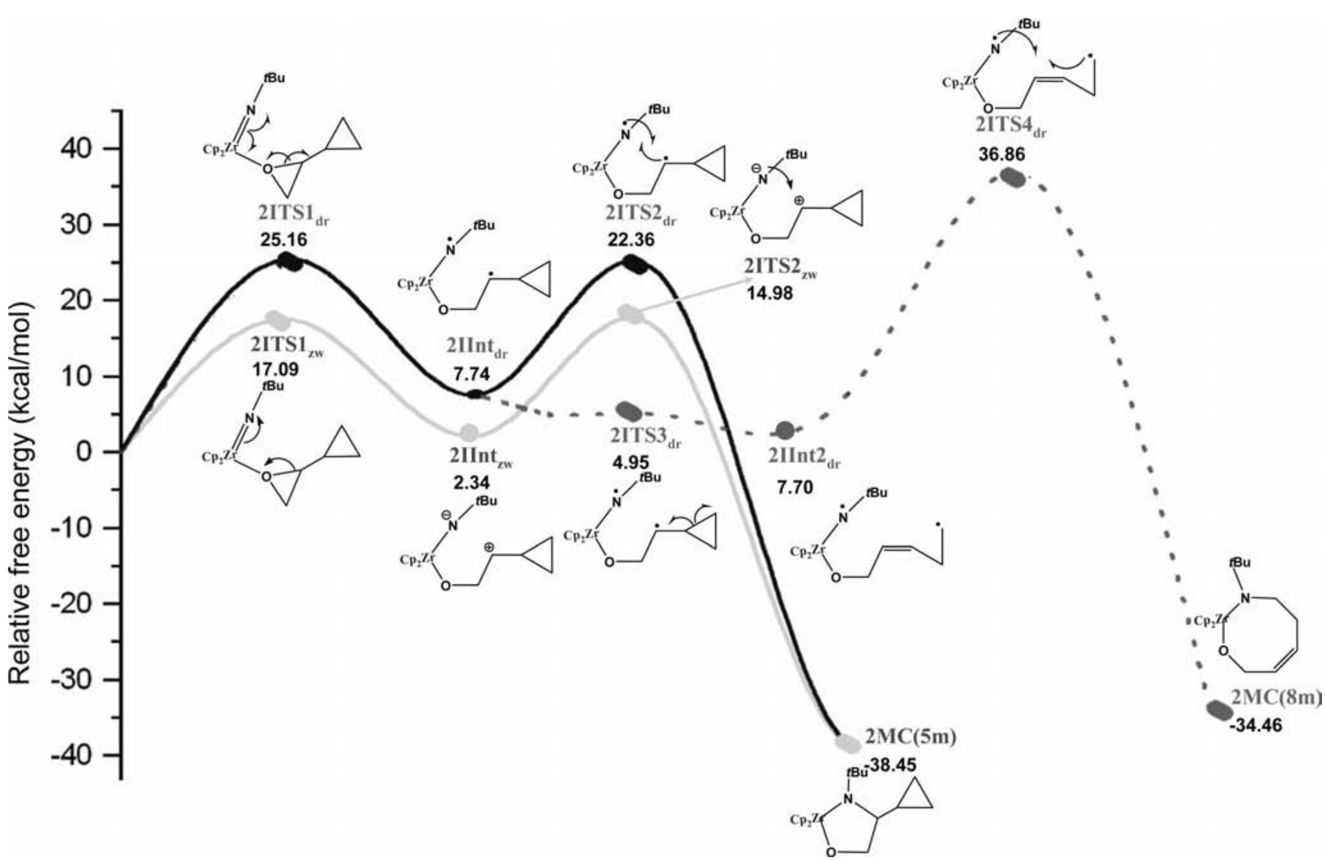

Figure 3. Free energy profile of ring cleavage reaction of **2** mediated by the imidozirconocene complex at B3LYP/LANL2DZ.

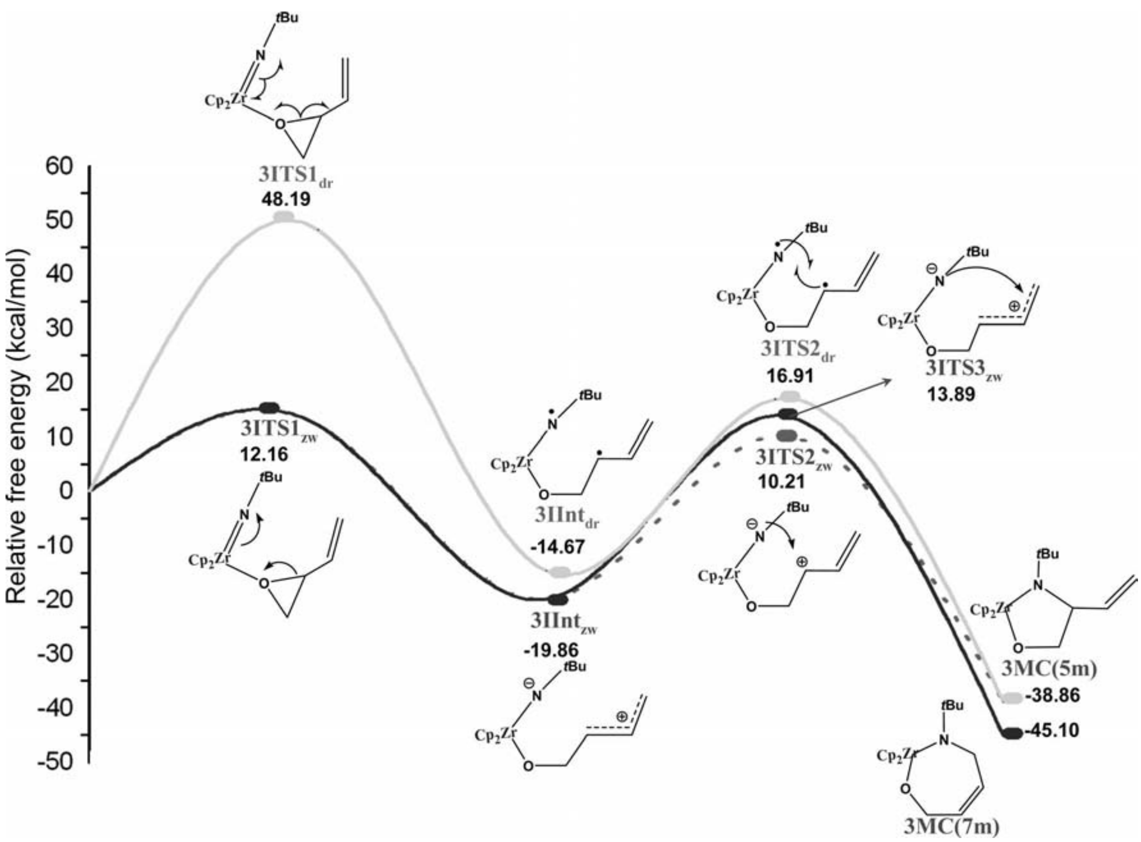

Figure 4. Relative free energy profile for the ring cleaving reaction of **3** mediated by the imidozirconocene complex (**4**) at the B3LYP/LANL2DZ level.

puted results. This reaction follows a zwitterionic path and involves two steps; the first step passes through **2**ITS1$_{zw}$ in which the C$_\alpha$–O bond is cleaved and the Zr←O coordination bond is converted into a covalent bond. The π electrons on the Zr=N bond are converted into a lone pair on the nitrogen atom, which leads to the formation of a zwitterionic intermediate **2**IInt$_{zw.}$ In the second step the C$_\alpha$–N bond is formed by the nucleophilic attack of the negative charge on the nitrogen atom on C$_\alpha$. This ring closing step is highly exothermic and stabilizes the product thermodynamically. The computed barriers suggest that the first step is rate determining. The zwitterionic intermediate **2**IInt$_{zw}$ is stabilized by the conjugation of the bent orbitals of the cyclopropane ring with the vacant p orbital of the cationic (C$_\alpha$) carbon atom.[47–48] The optimized geometries of the transition states (SI-4) show that the C$_\alpha$–O bond is partially broken in **2**ITS1$_{zw}$ and fully broken in **2**ITS2$_{zw}$. The Zr–N π bond is partially broken in **2**ITS2$_{zw}$ as the C$_\alpha$–N bond is formed.

Butadiene Monoepoxide (3)

In the imidozirconocene complex of **3**, the lone pair on **3** coordinates to the vacant orbital of the imidozirconocene complex through Zr←O coordination as seen above. The C$_\alpha$–O bond can cleave heterolytically or homolytically in the imidozirconocene reactant complex (RC). The heterolytic cleavage of the C$_\alpha$–O bond leads to a zwitterionic intermediate (**3**IInt$_{zw}$), and homolytic cleavage leads to a diradical intermediate (**3**IInt$_{dr}$).

The detailed mechanism is presented in Scheme 2 (R = 3). In this mechanism the zwitterionic intermediate (**3**IInt$_{zw}$) can lead to metallacyclic products in two ways, the formation of a five-membered [**3**MC(5m)] and a seven-membered metallacycle [**3**MC(7m)] through **3**ITS2$_{zw}$ and **3**ITS3$_{zw}$, respectively, are proposed. The relative free energy profile (Figure 4) clearly shows that the homolytic cleavage of the C$_\alpha$–O bond (**3**ITS1$_{zw}$) requires a high activation energy (48.19 kcal/mol) compared to the heterolytic cleavage in the first step, which rules out the possibility of diradical mechanism. The heterolytic C$_\alpha$–O cleavage leads to the formation of **3**IInt$_{zw}$, and this intermediate is more stable than the diradical intermediate (**3**IInt$_{dr}$). The stability of the zwitterionic intermediate (**3**IInt$_{zw}$) is attributed to the cation stabilization by the adjacent double bond, which is evident from the total valance non-Lewis contribution (3.28 %) obtained from NBO analysis. In this intermediate the positive charge is distributed along the allylic C$_\alpha$–C$_\beta$–C$_\gamma$ system. The product selectivity is based on the approach of the imidonucleophilic nitrogen atom towards the positively charged carbon atom (Scheme 2; R = 3). This nucleophilic attack depends on the localization of the positive charge around the allylic (C$_\alpha$–C$_\beta$–C$_\gamma$) carbon frame. The nucleophilic imido nitrogen atom attacks either the positively

 © 2011 Wiley-VCH Verlag GmbH & Co. KGaA, Weinheim

charged C_α or C_γ carbon atoms. The computed results indicate that the imido nitrogen atom predominantly attacks the C_α carbon atom and this is further confirmed by their Mulliken charges. The Mulliken charge at the C_α carbon atom (0.037) is higher and more positive than the Mulliken charge at the C_γ carbon atom (–0.548) in the zwitterionic intermediate. Generally the secondary carbocation (C_α) is more stable than the primary carbocation (C_γ), so the zwitterionic intermediate (**3**IInt$_{zw}$) leads to the formation of a five-membered **3**MC(5m) metallacycle through **3**ITS2$_{zw}$ over the seven-membered metallacycle **3**MC(7m). This is in agreement with experimental reports.[15] The optimized transition state geometries (SI-5) show that the Zr=N π bond is partially broken in **3**ITS1$_{zw}$ and completely broken in **3**ITS2$_{zw}$, as the Zr=N bond gradually lengthens. In the zwitterionic intermediate (**3**IInt$_{zw}$) the C_α–N bond is formed in **3**ITS2$_{zw}$. The relative free energy profile reveals that the zwitterionic pathway is predominant over the diradical pathway. In the zwitterionic pathway, five-membered metallacycle product formation is kinetically favorable due to the allylic stabilization of the carbocation.

Ring Cleavage of Epoxides with Accessible β-Hydrogen Atoms (4–6)

The presence of accessible hydrogen atoms at the β position opens up additional reaction pathways through elimination. Scheme 3 indicates that elimination is a one step process, whereas insertion is a two step reaction.

Only zwitterionic paths have been followed here as the diradical paths have been found to be energetically unfavorable in earlier cases and the detailed mechanism is provided in Scheme 3. As the mechanism is similar in all the three cases they are grouped for discussion. Insertion follows a two step mechanism and in the first step the zwitterionic intermediate is formed and this intermediate closes the ring forming a five-membered metallacycle. In the first transition state (**1**ITS1$_{zw}$–**6**ITS1$_{zw}$) of the insertion reaction, three changes are notable: (i) partial cleavage of C_α–O bond restoring the lone pair on the oxygen atom, (ii) partial conversion of the Zr←O bond to a Zr–O covalent bond, and (iii) partial breakage of the Zr=N π bond creating a second lone pair (negative charge) on the imido nitrogen atom. In the intermediate (**1**IInt$_{zw}$–**6**IInt$_{zw}$) these changes are effected fully and the charge centers are ready for ring closure. In the second step the negative charge on the imido nitrogen atom attacks the carbocation and the ring closes. This is similar to what has been observed with epoxides **1**–**3**. In elimination all bonding changes occur in one step, which leads to the formation of an allyl alkoxy product.

In addition to the three bonding changes followed in the first step of the insertion, three more bonding changes occur. The additional three steps are the formation of a N–H_β bond and cleavage of the C_α–H_β and C_α–C_β π bonds. This makes the complete transfer of a hydrogen atom resulting in the formation of the elimination product. The relative free energy profiles (see Figures 5, 6, and 7) show that the elimination path is low lying, involves a very low energy barrier, and the elimination product is thermodynamically more stable. Elimination is by far preferred with epoxides **4**–**6**, which is in total conformity with experimental observations.[15] The optimized geometries of the transition states and essential bond lengths also support the conclusions above (Figure S4 and S5).

Bifunctional Reactivity of Imidozirconocene Complex

Erker and coworkers[3] have reported the catalytic applications and bifunctional activity of zirconocene complexes. Grotjahn and coworkers[4] have reported the application of the bifunctional activity of iridium, ruthenium, and rhodium organometallic complexes in organic synthesis. In these reports, the origin of the bifunctional reactivity and the role of the metallocene molecular orbitals in the bifunctional reactivity have not been clearly discussed. In the present study Zr is found to act as a Lewis acid and the imido nitrogen atom acts as a Lewis base. Although this bifunctional reactivity has already been noted,[11,15] the involvement of specific molecular orbitals and other factors facilitating this bifunctional reactivity is still to be explored. This

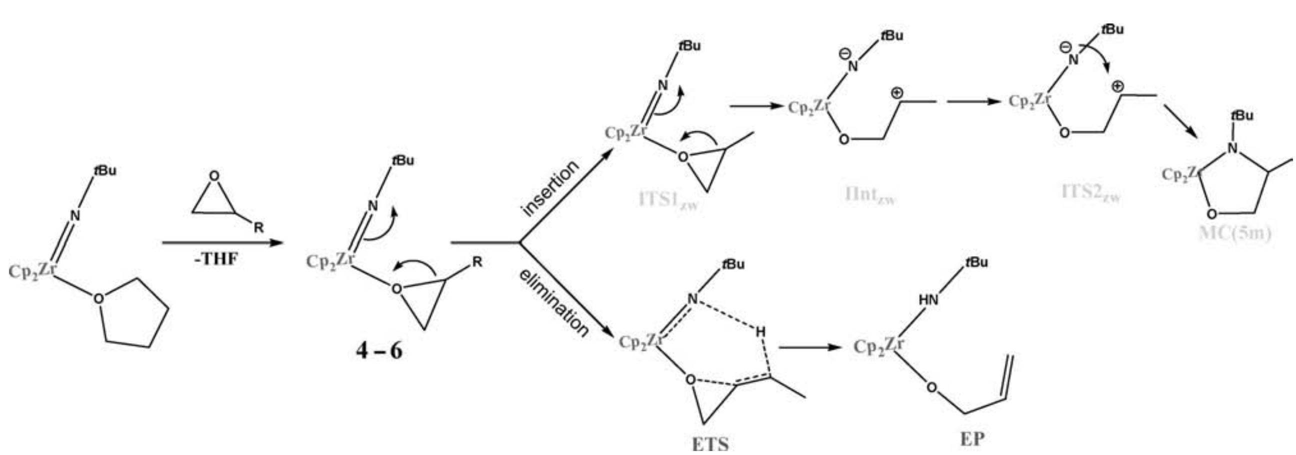

Scheme 3. Mechanism for the insertion and elimination pathways of epoxides **4**–**6** with accessible β-hydrogen atoms mediated by imidozirconocene.

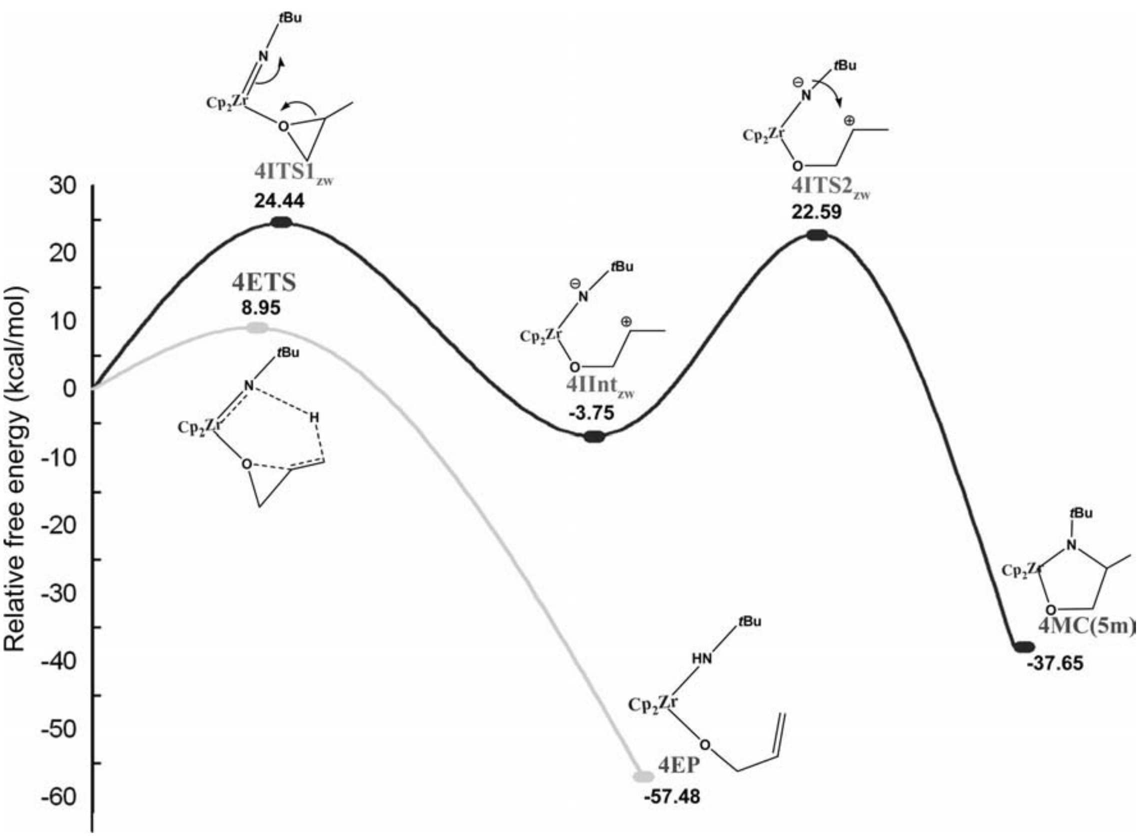

Figure 5. Relative free energy profile for the insertion and elimination reaction of **4** with the imidozierconocene complex at the B3LYP/LANL2DZ level.

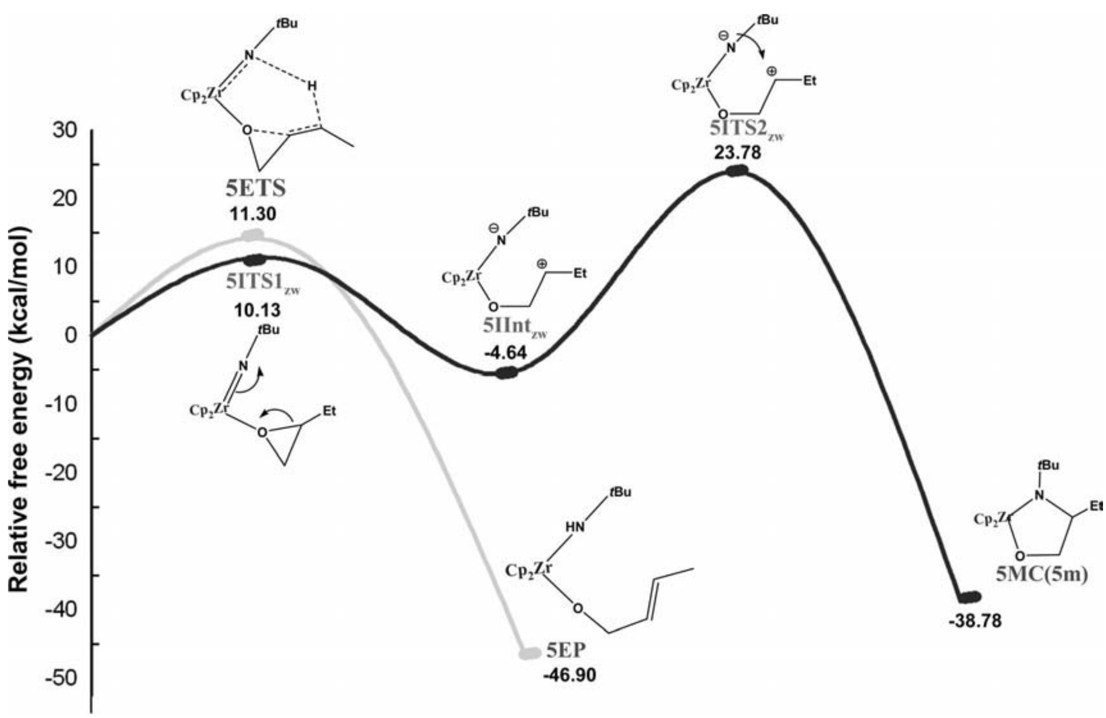

Figure 6. Relative free energy profile for the insertion and elimination reaction of **5** with the imidozirconocene complex at the B3LYP/LANL2DZ level.

work attempts to model the bifunctional reactivity in a quantitative way using EDA, NBO, and AIM topological analysis.

Epoxides form a complex initially through a coordinate bond between the oxygen lone pair and the vacant molecular orbital of the $Cp_2Zr{=}N{-}t$Bu fragment. In the next step

 © 2011 Wiley-VCH Verlag GmbH & Co. KGaA, Weinheim

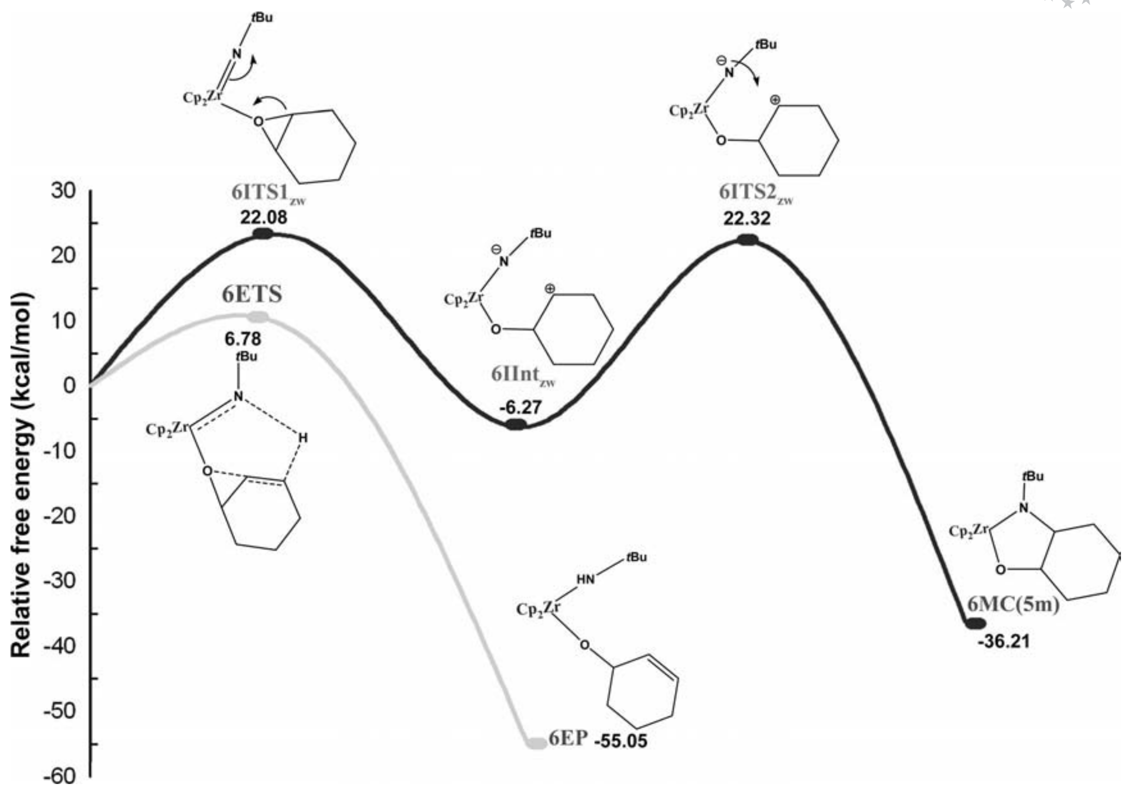

Figure 7. Relative free energy profile for the insertion and elimination reaction of **6** with the imidozierconocene complex at the B3LYP/LANL2DZ level.

Table 1. EDA at BP86/TZP of the imidozirconocene–epoxide complex (**1**RC–**6**RC) and insertion intermediates (**1**IInt$_{zw}$–**6**IInt$_{zw}$).[a]

	1RC	**1**Int$_{zw}$	**2**RC	**2**Int$_{zw}$	**3**RC	**3**Int$_{zw}$	**4**RC	**4**Int$_{zw}$	**5**RC	**5**Int$_{zw}$	**6**RC	**6**Int$_{zw}$
ΔE_{int}	–15.05	–628.64	–16.19	–124.99	–16.05	–312.38	–19.29	–353.97	–19.01	–103.52	–19.98	–50.41
ΔE_{Orb}	–17.84	–640.01	–18.29	–155.33	–20.54	–327.40	–20.11	–436.39	–19.79	–199.50	–20.78	–107.26
	(35.3)	(86.7)	(34.5)	(66.4)	(34.8)	(77.5)	(32.8)	(76.5)	(32.8)	(60.4)	(33.0)	(55.1)
ΔE_{Pauli}	35.37	109.79	36.79	108.89	42.99	110.21	42.02	216.79	41.23	226.54	43.03	143.28
ΔE_{Elstat}	–32.57	–98.43	–34.69	–78.55	–38.49	–95.19	–41.19	–134.36	–40.45	–130.55	–42.23	–86.44
	(64.7)	(13.7)	(65.5)	(33.6)	(65.3)	(22.5)	(67.2)	(23.5)	(67.2)	(39.6)	(67.0)	(44.9)
$\Delta E_{Elstat}/\Delta E_{Orb}$	1.82	0.15	1.89	0.50	1.87	0.29	2.04	0.30	2.04	0.65	2.03	0.80

[a] Energies in kcal/mol; the values in parentheses gives the percentage contribution to the total attractive interactions (ΔE_{Elstat} + ΔE_{Orb}).

this coordinate bond is converted into covalent bond by cleavage of the C_α–O bond. In the zwitterionic intermediate this coordinate bond is completely converted into covalent bond. In order to examine the conversion of the coordinate to covalent bond, EDA has been carried out for all the imidozirconocene epoxide RCs (**1**RC–**6**RC) and the intermediates of the insertion reaction (**1**IInt$_{zw}$–**6**IInt$_{zw}$) using BP86/TZP level and the results are presented in Table 1.

The computed interaction energies (ΔE_{int}) show that Cp_2Zr=N–*t*Bu and the epoxide fragment interact more strongly in the intermediate than in the RC. This leads to greater stabilization of the reaction intermediate than the RC. Calculated ΔE_{elstat} and ΔE_{Orb} values clearly indicate that the interaction between the two fragments is more electrostatic in the RC and more covalent in the intermediates. The $\Delta E_{elstat}/\Delta E_{Orb}$ ratio of the imidozirconoce RC (**1**RC–**6**RC) clearly reveals ($\Delta E_{elstat}/\Delta E_{Orb} > 1$) this fact and implies that the lone pair on the oxygen atom is donated to the vacant zirconium molecular orbital at the Cp_2Zr=N–*t*Bu fragment resulting in a coordinate Zr←O bond. This bond is converted into a full covalent bond ($\Delta E_{elstat}/\Delta E_{Orb} < 1$) in the reaction intermediate (**1**IInt$_{zw}$–**6**IInt$_{zw}$) as a result of series of electron migrations in the first step. The conversion of the zirconium–oxygen coordinate bond into a full covalent bond makes this bond shorter in the intermediate, which brings the two fragments closer. As a result ΔE_{Pauli} increases in the intermediate.

In the orbital correlation diagram (Figure 8) the imidozirconocene fragment (Cp_2Zr=N–*t*Bu) is considered as one fragment and the epoxide (**1**) is considered as the second fragment. According to the bent metallocene symmetry[11] approach, the Zr–N σ bond is formed primarily by the interaction of the imide orbital of a_1 symmetry with the $2a_1$ orbital of the Cp_2Zr fragment. The filled imide b_2 orbital

 © 2011 Wiley-VCH Verlag GmbH & Co. KGaA, Weinheim

interacts with the zirconium-based orbital of matching symmetry, giving rise to the *p*-component of the Zr–N bond. The third nitrogen-based orbital has b_1 symmetry and cannot interact with the remaining vacant a_1 orbital of the Cp_2Zr fragment.

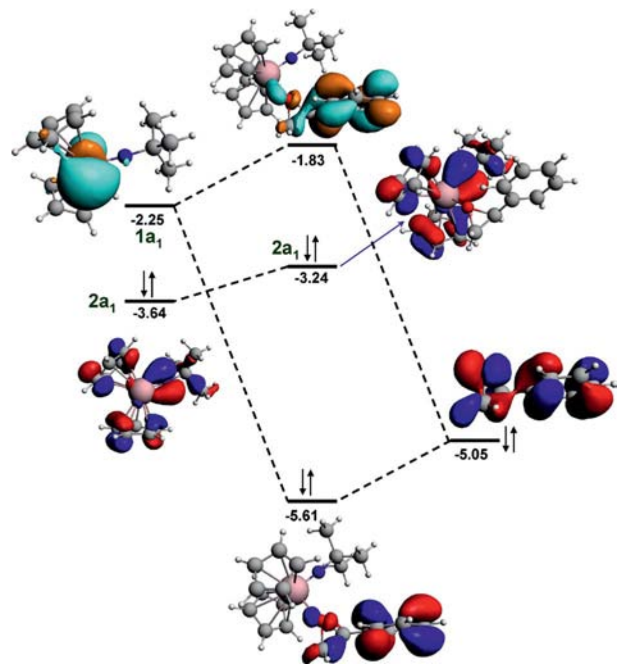

Figure 8. MO and energy [eV] level diagram for Cp_2Zr=N–*t*Bu–**1** RC.

The low lying metal-based orbital of a_1 symmetry is likely to play a pivotal role in accepting electron density from the dative epoxide imidozirconocene complex. The only available metal based orbital of b_1 symmetry is a high-lying orbital with Zr–Cp antibonding character. The vacant $2a_1$ orbital makes a π bond with the imide (=N–R) nitrogen atom and gives the Cp_2Zr=N–*t*Bu fragment. In this fragment two orbitals play a significant role in the bifunctional reactivity of the imidozirconium complex; one is a nonbonding $2a_1$ (flexible π bond) orbital and the other is the vacant $1a_1$ orbital. The empty $1a_1$ (σ symmetry) orbital accepts a pair of electrons from the epoxide lone pair and gives rise to the imidozirconocene RC. Another interesting observation is that the (π bonding symmetry) nonbonding $2a_1$ orbital energy is destabilized (up to 9.22 kcal/mol) from –3.64 to –3.24 eV. The destabilized $2a_1$ orbital (π bonding symmetry) is a nonbonding HOMO, which is centered on the imido nitrogen atom in the RC. This π bond ($2a_1$) converts into a single bond ($1a_1$) in **1**ITS1 to stabilize the metal coordination number and charge. In this way, the Lewis acidic Zr atom accepts a pair of electrons from the epoxide by which the $1a_1$ orbital of the Zr atom gets filled, which leads to simultaneous further destabilization of the $2a_1$ orbital. The energy increase of the $2a_1$ orbital leads to the breakage of the π bond (Zr=N), which results in the creation of a Lewis basic (negative charge) imido nitrogen atom. In this way the molecular orbital diagram (Figure 8) explains the bifunctional reactivity of the imidozirconocene complex in the epoxide ring cleavage reaction.

The second order perturbation energy analysis data are presented in Table 2. This table lists dominant orbital interactions in the RC, ITS1, and ITS2 in each of the reactions involving epoxides **1**, **2**, and **3** (Figure 9). In the RC, the interaction of the lone pair with the vacant d orbital of Zr (LP*) is found to be significant. In ITS1 only two interactions are found to be important; first is the interaction of $\sigma_{C\alpha\text{-}O}$ with LP*(O) and the second is the interaction of $\pi_{Zr=N}$ with $\pi^*_{Zr=N.}$ This first interaction indicates that the conversion of the C_α–O σ bond pair into a lone pair orbital on the oxygen atom, and the second interaction implies the π pair breakage and consequent creation of a lone pair on the imido nitrogen atom. As a result the Zr=N π bond is converted into to a Zr–N σ bond. The computed length of the Zr–N bond is shorter in the imidozirconocene complex than in ITS1, which provides evidence for the above (Table S1). In the intermediate, the C_β carbon atom makes a partial π bond with the carbocation (C_α) to stabilize the positive charge. In ITS2 the lone pair on the nitrogen atom interacts with the π* orbital of the C_α–C_β bond, which allows the migration of the negative charge (LP) to the imido nitrogen atom as a $\sigma_{N\text{–}C\alpha}$ bond pair.

Table 2. Second order perturbation interaction energy analysis for the TSs of the ring cleaving reaction involving epoxides **1**–**3** mediated by the imidozirconocene complex at B3LYP/LANL2DZ level.

Selected electronic interactions	**1**			**2**			**3**		
(energy, kcal/mol)	RC	TS1	TS2	RC	TS1	TS2	RC	TS1	TS2
O(LP) to Zr(LP*)	72.53	–	–	72.15	–	–	73.46	–	–
$\sigma_{C\alpha\text{-}O}$ σ to LP*(O)	–	16.58	–	–	16.69	–	–	15.58	–
$\pi_{Zr=N}$ to $\pi^*_{Zr=N}$(N)	–	15.12	–	–	10.56		–	9.46	–
N(LP) to $\pi^*_{C\alpha\text{-}C\beta}$	–	–	18.36	–	–	15.27	–	–	16.85

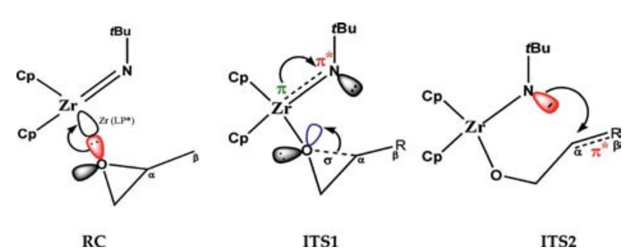

Figure 9. Various electronic interactions involved in ring cleaving TSs of insertion reaction of epoxides without accessible β-hydrogen atoms with the imidozirconocene complex.

In the elimination reaction, the zirconium and imido nitrogen atoms act concertedly as Lewis acid and Lewis base, respectively. Electronic reorganization takes place in a sin-

 © 2011 Wiley-VCH Verlag GmbH & Co. KGaA, Weinheim

gle step. Five electronic interactions were observed (Table 3) in the concerted TS structure. The second order perturbation energy analysis explains the electron migrations in a circuit (Figure 10).

Table 3. Second order perturbation interaction energy analysis for the TSs of the ring cleaving reaction involving epoxides **4**–**6** mediated by the imidozirconocene complex at B3LYP/LANL2DZ level.

Interactions (energy, [kcal/mol])	**4**ETS	**5**ETS	**6**ETS
O(LP) to Zr(LP*)	51.34	52.14	53.29
$\pi_{Zr=N}$(N) to $\pi^*_{Zr=N}$(N)	25.91	25.20	35.08
N(LP) to $\sigma^*_{C\beta\text{-}H}$	18.35	17.08	19.20
C_α–O (σ) to LP*(O)	9.46	7.68	7.80

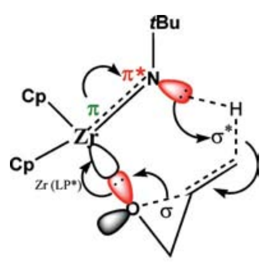

ETS

Figure 10. Various electronic interactions involved in proton shift TSs of elimination reaction of epoxides with accessible β-hydrogen atoms (**4**–**6**) with the imidozirconocene complex.

Topological Analysis of Insertion and Elimination Transition States

In order to gain further insight into the bonding situation and electron density distribution changes during the reaction, topological analysis has been carried out for the optimized geometries of RC, transition states, and intermediate of **1** and the elimination transition state of **4** using AIM analysis at the B3LYP/LANL2DZ level. The molecular graph with critical points and Laplacian of the electron density distribution [$\nabla^2\rho(r)$] at each critical point of the RC (**1**RC), transition states (**1**ITS1$_{zw}$ and **1**ITS2$_{zw}$), and intermediate (**1**IInt1$_{zw}$) of the insertion reaction are shown in Figure 11 and those for the elimination reaction are shown in Figure 12. In this Figure the bond critical points (3, –1; BCPs), ring critical points (3, +1; RCPs), and cage critical points (3, +3; CCPs) are printed in red, yellow, and green, respectively.

Invariably in all the cases the CCPs (3, +3) were located in between the Zr atom and the Cp ring, which shows the presence of a η^5-Zr (pπ-dπ) bond.

The molecular graph and Laplacian of the electron density distribution [$\nabla^2\rho(r)$] of **1**RC shows the electronic structure. The negative Laplacian ($\nabla^2 \rho_{BCP}$ = –0.063) of the BCP of the O–Zr bond shows that the O←Zr bond is coordinate (polar) rather than covalent. The domination of eigen values of Hessian λ_3 (0.35) compared to λ_1 (–0.05) and λ_2 (–0.05) at this critical point further support the existence of a coordinate bond (O←Zr) in **1**RC. In the Laplacian contour map of **1**RC, high charge depletion (C_{delp}) has been observed in the C_α–O bond direction (Figure 11), which shows that there is a high possibility for cleavage of the C_α–O bond in **1**RC. In the case of **1**ITS1$_{zw}$, the BCP of the Zr–O bond has a negative Laplacian value ($\nabla^2 \rho_{BCP}$ = –0.013), and these values are comparatively lower than that observed in **1**RC, which indicates that the Zr←O dative bond becomes a covalent bond in **I**TS1$_{zw}$.

The negative Laplacian value ($\nabla^2 \rho_{BCP}$ = –0.002) at the BCP of the Zr–O bond decreases in the intermediate (**1**IInt$_{zw}$) compared to that of **1**ITS1$_{zw}$, which confirms the transformation of the dative (Zr←O) bond to a Zr–O covalent bond. The Hessian eigen values also reflect the covalent bond conversion trend ($\lambda_1 \approx \lambda_2 > \lambda_3$). The availability of the carbocation in the intermediate (Figure 11) is further supported by the observation of charge depletion (C_{depl}) at the C_α carbon atom in the contour plot. The RCP (3, –1) is noted in the molecular graph (Figure 11), which confirms the ring closing nature of imido nitrogen atom with the C_α carbon atom. The BCP located between the imido nitrogen atom and the C_α carbon atom in **1**ITS2$_{zw}$ clearly supports the formation of a five-membered metallacycle in the insertion reaction. The absence of a RCP in **1**ITS1$_{zw}$ and **1**Int1$_{zw}$ supports the stepwise mechanism of ring cleavage of epoxides without β-hydrogen atoms with the imidozirconocene complex.

The molecular graph and Laplacian of the electron density distribution [$\nabla^2\rho(r)$] map for the elimination transition state (**4**ETS) of **4** is shown in Figure 12 (a), and the trajectory plot of the gradient vector field of the charge density of **4**ETS is shown in Figure 12 (b). The BCP (3, –1) located between the imido nitrogen atom and H_β undoubtedly reveals the formation of a partial H_β–N in the transition state. The negative value of Laplacian at this BCP ($\nabla^2\rho_{BCP}$ = –0.540) indicates that the possibility that H_β moves closer towards the nucleophilic imido nitrogen atom. The BCP of the O–Zr bond also has a negative Laplacian ($\nabla^2 \rho_{BCP}$ = –0.093) in the transition state but it is comparatively lower than that of the H_β–N_{imido} bond. The RCP (3, –1) is located (Figure 12, a) in the center of the six-membered H_β–C_β–C_α–O–Zr–N cyclic transition state of **4**ETS is proof of the intramolecular hydrogen transfer elimination reaction in a concerted path. Figure 12 (b) displays a gradient trajectory map of the total electron density in the transition state plane (**4**ETS), showing the BCPs and the bond path between the atoms involving the intermolecular hydrogen transfer transition state. The gradient trajectory map of the total electron density in the transition state depicted shows that the zero flux surface at C_β–H_β is highly associated with H_β. At the same time, the zero flux surface at H_β–N is highly associated with N compared to H_β (Figure 12, b). The gradient trajectory maps of the total electron density support the concerted elimination mechanism.

 © 2011 Wiley-VCH Verlag GmbH & Co. KGaA, Weinheim

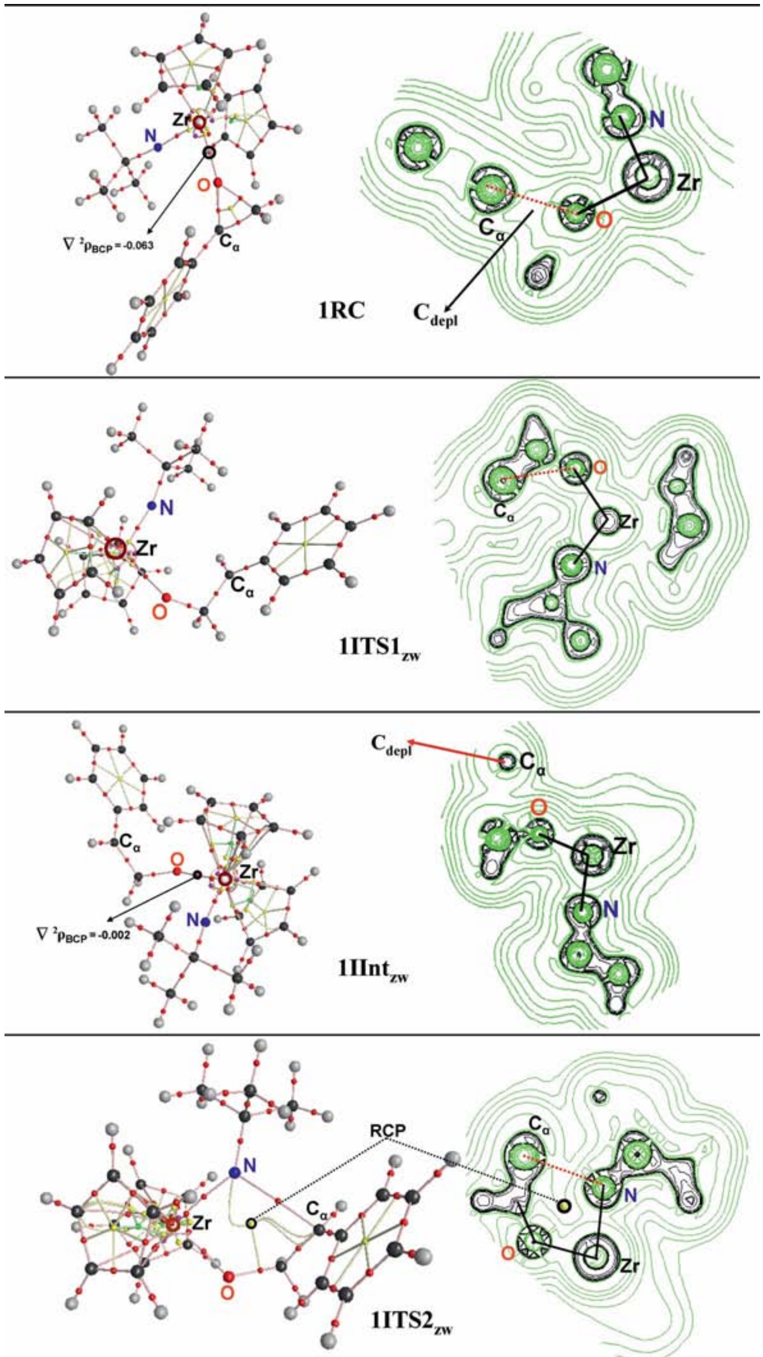

Figure 11. The molecular graph and contour map of reactant (IRC), insertion transition states (ITS1$_{zw}$ & ITS2$_{zw}$), insertion intermediate (IInt$_{zw}$) with bond critical point (BCP), ring critical point (RCP) and cage critical point (CCP).

Conclusions

Imidozirconocene-mediated ring cleavage of epoxides has been investigated using DFT calculations at the B3LYP/LANL2DZ level. Two types of epoxides have been employed, those without accessible β-hydrogen atoms (**1**–**3**) and those with (**4**–**6**). Epoxides **1**–**3** undergo only insertion, whereas **4**–**6** predominantly undergo elimination. The reactions of the imidozirconocene complex with **4**–**6** follow elimination reaction rather than insertion due to the availability of β-hydrogen atoms close to the nucleophilic imido nitrogen atom and activation of the accessible β-hydrogen atoms. The insertion reaction is a two step process in which the first step is rate determining, whereas elimination is a single step process. The computed results reveal that insertion prefers a zwitterionic path compared to a diradical path, which is due to the stabilization of the C_α carbocation through resonance, conjugative orbital interaction, and allylic stabilization. Invariably in all cases the C_α–O bond breaking in the imidozirconocene complex is the rate-de-

 © 2011 Wiley-VCH Verlag GmbH & Co. KGaA, Weinheim

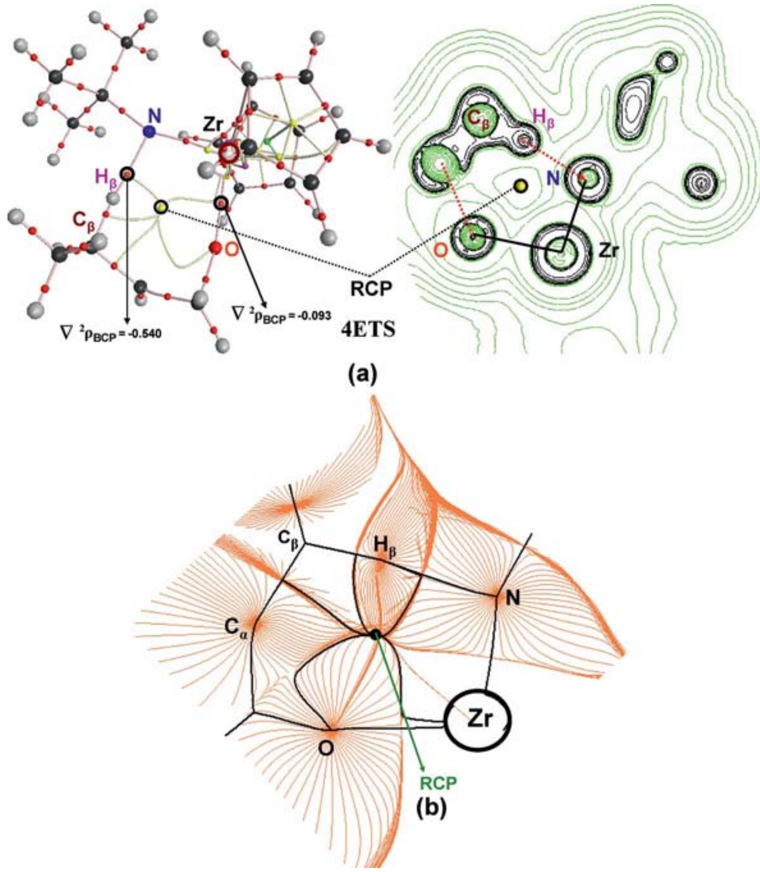

Figure 12. The view of molecular graph and contour map of elimination transition state (**4**ETS) with BCP, RCP, and CCP (a); trajectory plot of gradient victor field of the charge density of **4**ETS (b). In the trajectory plots black solid lines denotes bond paths and critical point paths; black solid circle denotes the ring critical point in **4**ETS.

termining step, which agrees with experimental findings.[15] In the imidozirconocene–epoxide complex, the lone pair on the oxygen atom is donated to the vacant molecular orbital of the zirconium atom (Lewis acidic center) in the Cp_2Zr=N–*t*Bu fragment, and in the first step the coordinate bond (Zr←O) is converted into a full covalent bond. At the same time the C_α–O bond is cleaved and the bond pair migrates as a lone pair on the oxygen atom, which makes a carbocation. These bonding changes around the Zr center induces a reorganization of the Zr=N bond into a Zr–N bond and the π bond pair is converted to an additional lone pair on the nitrogen atom making N^- (Lewis base). As a result a zwitterionic intermediate is formed, in which the N^- attacks the C_α carbocation leading to a thermodynamically stable five-membered metallacycle. The proposed seven- and eight-membered metallacycle formation proposed previously[14] in the case of **2** and **3** is found to be unfeasible. In the elimination reaction, all bonding changes occur concertedly in single step. The availability of β-hydrogen atoms facilitates simultaneous proton transfer to the anionic imido nitrogen atom creating a C_α–C_β π bond.

EDA analysis clearly explains the electronic structure and existing bonding nature between the imidozirconocene and epoxide fragments in the imidozirconocene–epoxide RC. The $\Delta E_{\mathrm{Elstat}}/\Delta E_{\mathrm{Orb}}$ ratio explains that the existing bond is the coordinate bond between the imidozirconocene complex and the epoxidic oxygen lone pair in the imidozirconocene RC. The conversion of the coordinate bond into a covalent bond is a consequence of the cleavage of the C_α–O bond. The higher $\Delta E_{\mathrm{Elstat}}$ contribution to attractive interaction in the imidozirconocene RC and the ΔE_{Orb} contribution to attractive interaction in the insertion intermediate strongly supports the conversion of the coordinate to a covalent bond. The Lewis acidic interaction of the imidozirconocene fragment makes an initial coordination to the epoxide through the vacant metal $1a_1$ orbital of the Cp_2Zr=N–*t*Bu fragment with a lone pair of electrons on the epoxide oxygen atom. As a result of this coordination, the π bonded $2a_1$ orbital energy increases. The coordination of $1a_1$ with the epoxide lone pair leads to the conversion of the Zr=N π bond to a Zr–N σ bond. The second order perturbation energy analysis also supports the various electronic migrations in the transition states. In the case of epoxides with accessible β-hydrogen atoms, the electron flow through bond breaking and bond making in a concerted manner is evident from second order perturbation analysis. In this case the imidozirconocene complex acts as both a Lewis acid and Lewis base. Furthermore, the stepwise mechanism of the insertion reaction for the first type of epoxide and concerted elimination mechanism for the second type with the imidozirconocene complex was confirmed by bond and ring critical points and contour plots of transition states obtained through AIM analysis.

Supporting Information (see footnote on the first page of this article): Details of the EDA and broken-symmetry formalisms used and structures along with Cartesian coordinates of all reactant complexes, transition states, intermediates and products.

Acknowledgments

We thank the Council of Scientific & Industrial Research (CSIR), India for financial support (research grant number 02 (2158)/07/EMR-II). Support from Professor Gernot Frenking (Philipps University Marburg, Germany), the Deutsche Forschungsgemeinschaft (DFG), and the Indian National Science Academy to P. V. for an exchange visit to Marburg in 2003 is gratefully acknowledged.

[1] a) W. A. Nugent, B. L. Haymore, *Coord. Chem. Rev.* **1980**, *31*, 123–175; b) W. A. Nugent, J. M. Mayer, *Metal-Ligand Multiple Bonds*, Wiley Interscience, New York, **1988**; c) D. E. Wigley, *Prog. Inorg. Chem.* **1994**, *42*, 239; d) P. Mountford, *Chem. Commun.* **1997**, 2127–2134; e) C. C. Romao, F. E. Kuhn, W. A. Herrmann, *Chem. Rev.* **1997**, *97*, 3197–3246; f) A. A. Danopoulos, J. C. Green, M. B. Hursthouse, *J. Organomet. Chem.* **1999**, *591*, 36–44; g) R. R. Schrock, *Tetrahedron* **1999**, *55*, 8141–8153; h) T. R. Cundari, *Chem. Rev.* **2000**, *100*, 807–818; i) P. R. Sharp, *J. Chem. Soc., Dalton Trans.* **2000**, 2647–2657; j) R. R. Schrock, *J. Chem. Soc., Dalton Trans.* **2001**, 2541–2550; k) L. H. Gade, P. Mountford, *Coord. Chem. Rev.* **2001**, *216–217*, 65–97; l) A. P. Duncan, R. G. Bergman, *Chem. Rec.* **2002**, *2*, 431–445; m) R. A. Eikey, M. M. Abu-Omar, *Coord. Chem. Rev.* **2003**, *243*, 83–124; n) W. H. Leung, *Eur. J. Inorg. Chem.* **2003**, 583–593.

[2] a) D. Pattenden, in: *Comprehensive Organic Synthesis*, Pergamon, Oxford, **1991**, *13*, p. 733; b) G. H. Posner, J. P. Maxwell, M. J. Kahraman, *Org. Chem.* **2003**, *68*, 3049–3054; c) I. M. Pastor, M. Yus, *Curr. Org. Chem.* **2005**, *9*, 1–29.

[3] a) G. Erker, *Acc. Chem. Res.* **2001**, *34*, 309–317; b) G. Erker, W. Fromberg, C. Kruger, E. Raabe, *J. Am. Chem. Soc.* **1988**, *110*, 2400–2405; c) M. Dahlmann, G. Erker, K. Bergander, *J. Am. Chem. Soc.* **2000**, *122*, 7986–7998; d) J. W. Strauch, J. Faure, S. Bredeau, C. Wang, G. Kehr, R. Fröhlich, R. Luftmann, G. Erker, *J. Am. Chem. Soc.* **2004**, *126*, 2089–2104; e) M. Hill, G. Erker, G. Kehr, R. Fröhlich, O. Kataeva, *J. Am. Chem. Soc.* **2004**, *126*, 11046–11057; f) J. Ugolotti, G. Kehr, R. Fröhlich, S. Grimme, G. Erker, *J. Am. Chem. Soc.* **2009**, *131*, 1996–2007; g) C. Valero, M. Grehl, D. Wingbermale, L. Kloppenburg, D. Carpenetti, G. Erker, J. L. Petersen, *Organometallics* **1994**, *13*, 415–417; h) R. Gleiter, I. Hyla-Kryspin, S. Niu, G. Erkert, *Organometallics* **1993**, *12*, 3828–3836.

[4] a) V. Miranda-Soto, D. B. Grotjahn, A. G. DiPasquale, A. L. Rheingold, *J. Am. Chem. Soc.* **2008**, *130*, 13200–13201; b) G. Erdogan, D. B. Grotjahn, *J. Am. Chem. Soc.* **2009**, *131*, 10354–10355; c) D. B. Grotjahn, X. Zeng, A. L. Cooksy, S. Kassel, A. G. DiPasquale, L. N. Zakharov, A. L. Rheingold, *Organometallics* **2008**, *27*, 3626; d) D. B. Grotjahn, V. Miranda-Soto, E. J. Kragulj, D. A. Lev, G. Erdogan, X. Zeng, A. L. Cooksy, *J. Am. Chem. Soc.* **2008**, *130*, 20–21.

[5] a) M. P. Shaver, M. D. Fryzuk, *Adv. Synth. Catal.* **2003**, *345*, 1061–1076; b) D. E. Wigley, *Prog. Inorg. Chem.* **1994**, *42*, 239–482.

[6] M. H. Chisholm, I. P. Rothwell, in: *Comprehensive Coordination Chemistry*, G. Wilkinson, R. D. Gillard, J. A. McCleverty, Pergamon Press, Oxford, England, **1987**, *2*, p. 161–188.

[7] G. Bartoli, M. Bosco, A. Carlone, M. Locatelli, M. Massaccesi, P. Melchiorre, L. Sambri, *Org. Lett.* **2004**, *6*, 2173–2176.

[8] J. F. Larrow, S. E. Schaus, E. N. Jacobsen, *J. Am. Chem. Soc.* **1996**, *118*, 7420–7421.

[9] M. Caron, K. B. Sharpless, *J. Org. Chem.* **1985**, *50*, 1557–1560.

[10] S. C. Bergmeier, *Tetrahedron* **2000**, *56*, 2561–2576.

[11] D. J. Ager, I. Prakash, D. R. Schaad, *Chem. Rev.* **1996**, *96*, 835–876.

[12] E. Ichikawa, M. Suzuki, K. Yabu, M. Albert, M. Kanai, M. Shibasaki, *J. Am. Chem. Soc.* **2004**, *126*, 11808–11809.

[13] J. J. Kennedy-Smith, K. A. Nolin, H. P. Gunterman, F. D. Toste, *J. Am. Chem. Soc.* **2003**, *125*, 4056–4057.

[14] S. E. Eldred, D. A. Stone, S. H. Gellman, S. S. Stahl, *J. Am. Chem. Soc.* **2003**, *25*, 3422–3423.

[15] S. A. Blum, V. A. Rivera, R. T. Ruck, F. E. Michael, R. G. Bergman, *Organometallics* **2005**, *24*, 1647–1659.

[16] A. Gansauer, T. Lauterbach, S. Narayan, *Angew. Chem. Int. Ed.* **2003**, *42*, 5556–5573.

[17] S. Shaik, H. Hirao, D. Kumar, *Acc. Chem. Res.* **2007**, *40*, 532–542.

[18] R. J. Enemærke, G. H. Hjøllund, K. Daasbjerg, T. C. Skrydstrup, *C. R. Acad. Sci., Ser. IIc* **2001**, *4*, 435.

[19] Y. Handa, J. Inanaga, *Tetrahedron Lett.* **1987**, *28*, 5717–5718.

[20] S. A. Blum, P. J. Walsh, R. G. Bergman, *J. Am. Chem. Soc.* **2003**, *125*, 14276–14277.

[21] M. J. Frisch, G. W. Trucks, H. B. Schlegel, G. E. Scuseria, M. A. Robb, J. R. Cheeseman, J. A. Montgomery Jr., T. Vreven, K. N. Kudin, J. C. Burant, J. M. Millam, S. S. Iyengar, J. Tomasi, V. Barone, B. Mennucci, M. Cossi, G. Scalmani, N. Rega, G. A. Petersson, H. Nakatsuji, M. Hada, M. Ehara, K. Toyota, R. Fukuda, J. Hasegawa, M. Ishida, T. Nakajima, Y. Honda, O. Kitao, H. Nakai, M. Klene, X. Li, J. E. Knox, H. P. Hratchian, J. B. Cross, V. Bakken, C. Adamo, J. Jaramillo, R. Gomperts, R. E. Stratmann, O. Yazyev, A. J. Austin, R. Cammi, C. Pomelli, J. W. Ochterski, P. Y. Ayala, K. Morokuma, G. A. Voth, P. Salvador, J. J. Dannenberg, V. G. Zakrzewski, S. Dapprich, A. D. Daniels, M. C. Strain, O. Farkas, D. K. Malick, A. D. Rabuck, K. Raghavachari, J. B. Foresman, J. V. Ortiz, Q. Cui, A. G. Baboul, S. Clifford, J. Cioslowski, B. B. Stefanov, G. Liu, A. Liashenko, P. Piskorz, L. Komaromi, R. L. Martin, D. J. Fox, T. Keith, M. A. Al-Laham, C. Y. Peng, A. Nanayakkara, M. Challacombe, P. M. W. Gill, B. Johnson, W. Chen, M. W. Wong, C. Gonzalez, J. A. Pople, *Gaussian 03*, revision B.04, Gaussian, Inc., Pittsburgh, PA, **2003**.

[22] a) P. J. Hay, J. Wadt, *J. Chem. Phys.* **1995**, *82*, 2154–5461; b) P. J. Hay, J. Wadt, *J. Chem. Phys.* **1985**, *82*, 70; c) j. Wadt, P. J. Hay, *J. Chem. Phys.* **1985**, *82*, 284; d) P. J. Hay, J. Wadt, *J. Chem. Phys.* **1985**, *82*, 299.

[23] a) C. Y. Zhao, D. Q. Wang, D. L. Phillips, *J. Am. Chem. Soc.* **2003**, *125*, 15200–15209; b) Z. Y. Lin, L. Dang, *Organometallics* **2008**, *27*, 4443–4454; c) B. C. Boren, S. Narayan, L. K. Rasmussen, L. Zhang, H. T. Zhao, Z. Y. Lin, G. C. Jia, V. V. Fokin, *J. Am. Chem. Soc.* **2008**, *130*, 8923–8930; d) H. Z. Yu, G. C. Jia, Z. Y. Lin, *Organometallics* **2009**, *28*, 1158–1164.

[24] M. A. Bach, P. Parameswaran, E. D. Jemmis, U. Rosenthal, *Organometallics* **2007**, *26*, 2149–2156.

[25] E. D. Jemmis, A. K. Phukan, K. T. Giju, *Organometallics* **2002**, *21*, 2254–2261.

[26] E. D. Jemmis, S. Roy, V. V. Burlakov, H. Jiao, M. Klahn, S. Hansen, U. Rosenthal, *Organometallics* **2010**, *29*, 76–81.

[27] a) K. Fukui, *J. Phys. Chem.* **1970**, *74*, 416–4163; b) K. Fukui, *Acc. Chem. Res.* **1981**, *14*, 363–368; c) C. Gonzalez, H. B. Schlegel, *J. Chem. Phys.* **1989**, *90*, 2154–2161.

[28] E. D. Glendening, A. E. Reed, J. E. Carpenter, F. Weinhold, *NBO*, version 3.1.

[29] A. E. Reed, L. A. Curtiss, F. Weinhold, *Chem. Rev.* **1988**, *88*, 899–926.

[30] a) L. Noodleman, *J. Chem. Phys.* **1981**, *74*, 5737; b) L. Noodleman, E. J. Baerends, *J. Am. Chem. Soc.* **1984**, *106*, 2316–2327; c) L. Noodleman, C. Y. Peng, D. A. Case, J. M. Mouesca, *Coord. Chem. Rev.* **1995**, *144*, 199–244.

 © 2011 Wiley-VCH Verlag GmbH & Co. KGaA, Weinheim

[31] V. Bachler, P. Chaudhuri, K. Wieghardt, *Chem. Eur. J.* **2001**, *7*, 404.
[32] a) K. Yamaguchi, Y. Takahara, T. Fueno, K. Nasu, *Jpn. J. Appl. Phys.* **1987**, *26*, L1362–L1364; b) K. Yamaguchi, F. Jensen, A. Dorigo, K. N. Houk, *Chem. Phys. Lett.* **1988**, *149*, 537–542; c) K. Yamaguchi, Y. Takahara, T. Fueno, K. N. Houk, *Theor. Chim. Acta* **1988**, *73*, 337.
[33] G. De Velde, F. Bickelhaupt, E. J. Baerends, S. A. J. van Gisbergen, G. C. Fonseca, J. G. Snijders, T. Ziegler, *J. Comput. Chem.* **2001**, *22*, 931–967.
[34] C. F. Guerra, J. G. Snijders, G. De Velde, E. Baerends, *J. Theor. Chim. Acc.* **1998**, *99*, 391–403.
[35] Amsterdam Density Functional, SCM, Vrije Universiteit, Amsterdam, The Netherlands; http://www.scm.com.
[36] J. P. Perdew, K. Burke, M. Ernzerhof, *Phys. Rev. Lett.* **1996**, *77*, 3865–3868.
[37] E. van Lenthe, E. J. Baerends, J. G. Snijders, *J. Chem. Phys.* **1993**, *99*, 4597–4610.
[38] E. van Lenthe, E. J. Baerends, J. G. Snijders, *J. Chem. Phys.* **1994**, *101*, 9783–9792.
[39] E. van Lenthe, A. E. Ehlers, E. J. Baerends, *J. Chem. Phys.* **1999**, *110*, 8943–8953.
[40] K. Morokuma, *J. Chem. Phys.* **1971**, *55*, 1236–1244.
[41] T. Ziegler, A. Rauk, *Theor. Chim. Acta* **1977**, *46*, 1–10.
[42] M. Lein, J. Frunzke, A. Timoshkin, G. Frenking, M. Lein, *Inorg. Chem.* **2003**, *42*, 2504–2511.
[43] R. F. W. Bader, *Atoms in Molecules: A Quantum Theory*, Oxford University Press, Oxford, UK, **1990**.
[44] R. F. W. Bader, *J. Phys. Chem. A* **1998**, *102*, 7314–7323.
[45] R. F. W. Bader, *J. Phys. Chem. A* **2009**, *113*, 10391–10396.
[46] A. Kovacs, C. Esterhuysen, G. Frenking, *Chem. Eur. J.* **2005**, *11*, 1813–1825.
[47] B. Saha, L. Mei-Huey, T. V. RajanBabu, *J. Org. Chem.* **2007**, *72*, 8648–8655.
[48] a) R. B. Martin, *J. Am. Chem. Soc.* **1970**, *92*, 1660–1666; b) E. Namanworth, *J. Am. Chem. Soc.* **1970**, *92*, 3234–3235; c) V. Buss, R. Gleiter, P. v. R. Schleyer, *J. Am. Chem. Soc.* **1971**, *93*, 3927–3933; P. Spillner, *J. Am. Chem. Soc.* **1974**, *96*,7591–7593.

Received: February 5, 2011
Published Online: May 17, 2011

 © 2011 Wiley-VCH Verlag GmbH & Co. KGaA, Weinheim